

## Observations of meridional scale frequency dependence in the coupled tropical ocean-atmosphere system

Chunzai Wang and Robert H. Weisberg

Department of Marine Science, University of South Florida, St. Petersburg

**Abstract.** It is generally observed in models of the coupled tropical ocean-atmosphere system that the meridional scales for oscillations at interannual periods are larger than an oceanic equatorial Rossby radius of deformation. Using 9 years of the high-resolution optimum interpolation sea surface temperature (SST) product of the National Oceanic and Atmospheric Administration (NOAA)/National Centers for Environmental Prediction (NCEP), analyses are made on the frequency dependence of the observed meridional scales, with emphasis on the latitudinal structures in the central Pacific at 140°W. On the relatively short intraseasonal and seasonal timescales the SST variations are found to occur over a meridional scale of the oceanic equatorial Rossby radius of deformation suggested by conventional equatorially trapped wave theory. In contrast to this, on the longer annual and interannual timescales the meridional scales are found to increase beyond the oceanic equatorial Rossby radius of deformation. A physical explanation for this meridional scale increase with decreasing frequency in the coupled tropical ocean-atmosphere system is discussed.

### 1. Introduction

Coupled ocean-atmosphere models, from the simplest linear perturbation models [e.g., Hirst, 1988; Wang and Weisberg, 1994a] to the intermediate models [e.g., Zebiak and Cane, 1987] and the most complicated general circulation models [e.g., Barnett et al., 1991; Chao and Philander, 1993; Latif and Barnett, 1995], all show meridional scales for coupled oscillations that are larger than the oceanic equatorial Rossby radius of deformation. This meridional scale broadening in the ocean with respect to the El Niño-Southern Oscillation (ENSO) is also an observed property of western Pacific thermocline anomalies [e.g., White et al., 1987, 1989; Kessler, 1990] and of eastern Pacific sea surface temperature (SST) anomalies [e.g., Wang and Weisberg, 1996]. Kessler and McPhaden [1995] also highlight such low-frequency behavior for the 20°C isotherm in the Tropical Atmosphere-Ocean array data.

With simplifying assumptions applied to the coupled ocean-atmosphere system, Wang and Weisberg [1994b, 1996] found analytical solutions for coupled equatorial wave modes having the property that their meridional scales increase with decreasing frequency. At high frequency these equatorial wave modes are not affected by air-sea coupling, so their meridional scale conforms to an oceanic equatorial Rossby radius of deformation. At low frequency these equatorial wave modes are affected by coupling, and as a result, their phase speeds are decreased, and their meridional scales are larger than an oceanic equatorial Rossby radius of deformation. A simple explanation for this follows from the intrinsic scale difference between the ocean and the atmosphere. Conceptually, for a coupled ocean-atmosphere system with two intrinsically different meridional scales the meridional scale of coupled modes should take on an intermediate value between the scales of the ocean and the atmosphere. Physically, the addition of an

ocean-atmosphere coupling-induced wind stress curl to the vorticity equation, as an external torque, alters the dispersion relationship for the equatorial waves. Without wind stress curl, gradients in buoyancy and planetary vorticity are the intrinsic environmental properties that determine the meridional scale. With wind stress curl an additional coupling parameter must be added which broadens the meridional scale. The present paper develops observational evidence of such oceanic meridional scale broadening using a high-resolution sea surface temperature (SST) product.

### 2. Data

An optimum interpolation (OI) global SST data set produced weekly on a 1° longitude by 1° latitude grid is available from the NOAA National Centers for Environmental Prediction (NCEP). This OI SST product uses in situ (ship and buoy) SST data, satellite SST retrievals, and data on sea-ice coverage, and a detailed description is given by Reynolds and Smith [1994, 1995]. The high-resolution OI SST product resolves equatorial upwelling and fronts much better than the previous low-resolution blended SST product [Reynolds and Smith, 1995], and it provides an excellent medium for analyzing the meridional structures of the ocean-atmosphere system as manifest in SST.

The OI SST along 140°W between 20°N and 20°S is used for studying meridional scales of the tropical ocean-atmosphere system. The SST as a function of latitude and time along 140°W is shown in Figure 1, where the data have been low-pass filtered using a truncated Fourier transform to remove oscillations occurring on timescales shorter than monthly. The contour interval is 1°C, and shading denotes SST larger than 27°C with the darkest regions larger than 29°C. All of the major features in the tropical Pacific, the equatorial cold tongue and the manifestations of the Intertropical Convergence Zone (ITCZ) and the South Pacific Convergence Zone (SPCZ), are evident.

On average, the coldest waters are located about the equa-

Copyright 1998 by the American Geophysical Union.

Paper number 97JC02722.  
0148-0227/98/97JC-02722\$09.00

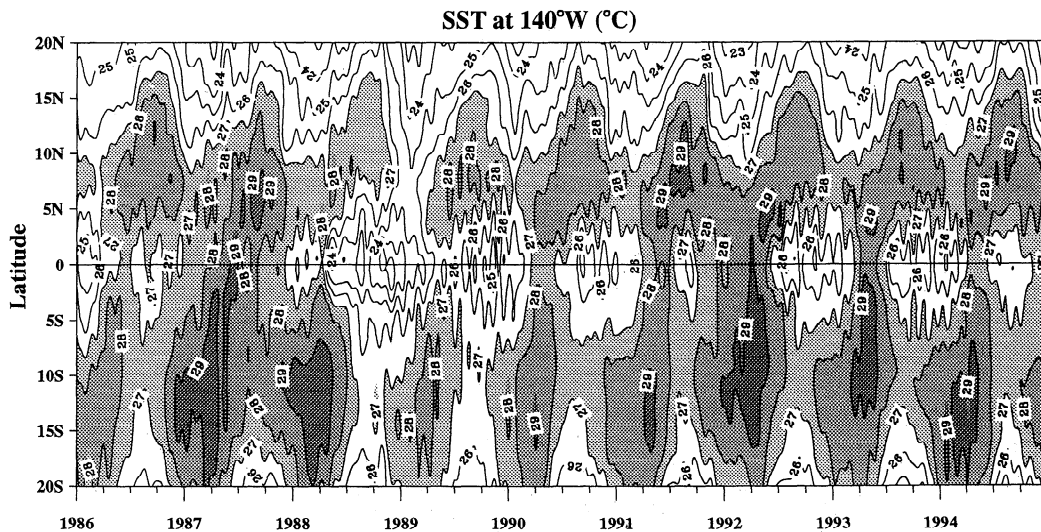


**Figure 1.** Sea surface temperature (SST) as a function of latitude and time along 140°W. The data have been low-pass filtered using a truncated Fourier transform to remove oscillations at timescales shorter than monthly. The contour interval is 1°C, and shading denotes SST larger than 27°C with the darkest regions larger than 29°C.

tor, and the warmest waters associated with the ITCZ and SPCZ are centered at about 8°N and 12°S, respectively. Both the ITCZ and the SPCZ, as well as the equatorial cold tongue, display an annual cycle. The ITCZ is stronger (weaker) and northernmost (southernmost) to the equator in the boreal summer/fall transition (winter/spring), whereas the SPCZ is stronger (weaker) and southernmost (northernmost) to the equator in the boreal winter/spring transition (summer/fall). The equatorial cold tongue is most developed in boreal fall, whereas it is least developed in boreal spring. The physical processes that control these annual SST variations associated with hemispheric climate asymmetry are complicated, and their relative importances must differ spatially. For example, Chang [1996] demonstrated that variations in the coupled ocean-atmosphere system can be divided into a forced solar radiation part and a dynamical ocean-atmosphere feedback part. The latter part contributes significantly to the pronounced annual cycle in the eastern Pacific but is less influential in the western Pacific owing to the different climate mean conditions. Other investigators have also argued that both ocean dynamical processes and surface heat fluxes are responsible for the annual cycle in the eastern Pacific [e.g., Hayes *et al.*, 1991; Chang, 1993; Xie and Philander, 1994; Xie, 1994], and in a coupled general circulation model study, Philander *et al.* [1996] pointed out that a positive feedback between low-level stratus clouds and cold SST can amplify a preexisting hemispheric climate asymmetry in both the eastern Pacific and Atlantic Oceans.

Despite the complex nature of tropical SST variations, certain generalizations apply. Outside the equatorial band, the annual cycle in SST conforms to annual solar radiation forcing modified by underlying wind-forced ocean dynamics. The antisymmetric annual variations in solar radiation relative to the equator, for instance, cause the antisymmetry in SST between the northern and southern hemispheres. Solar radiation on the equator, however, is dominated by a semiannual cycle since the Sun passes the equator twice a year (neglecting variations of the cloudiness). The large annual cycle in equatorial SST sug-

gests that ocean dynamical processes (e.g., equatorial upwelling and vertical mixing, horizontal advection and eddy heat flux convergence) may also be important. There are recent model studies pointing out the possible complementary roles of surface heat flux in the seasonal cycle of equatorial SST. For example, Li and Philander [1996] showed that the seasonally varying solar radiation along with the asymmetry of the time-averaged climate conditions can produce a modest amplitude of an SST annual cycle on the equator and that the oceanic dynamical response further augments this modest annual cycle to achieve a realistic amplitude. Note that during the annual transition from southern hemisphere to northern hemisphere, warm SST contours are nearly continuous across the equator following the march of the Sun since, during that time, equatorial upwelling is weak and SST is mainly controlled by solar radiation. However, during the reverse march of the Sun (from the northern hemisphere to the equator to the southern hemisphere), the SST contours are discontinuous since equatorial upwelling then dominates the equatorial SST variations. Since the SST and the wind influence each other via ocean-atmosphere coupling, interannually, during the warm phases of ENSO (e.g., the 1986–1987 and 1991–1992 periods of El Niño) the equatorial cold tongue is weakened or disappears when both the ITCZ and the SPCZ move toward and merge around the equator and conversely during the cold phase of ENSO (e.g., the 1988–1989 La Niña).

### 3. Frequency Dependence of Meridional Scale

With SST varying over different timescales from intraseasonal to interannual we define an anomaly field and then analyze the meridional structure of the anomalies as a function of timescale. The overall anomaly field at 140°W, which was calculated by subtracting the time-averaged SST at each latitude from the SST variability of Figure 1, is shown in Figure 2 as a function of latitude and time. These anomalies were further separated into intraseasonal to interannual bands by band-pass filtering. Intraseasonal band is defined to include

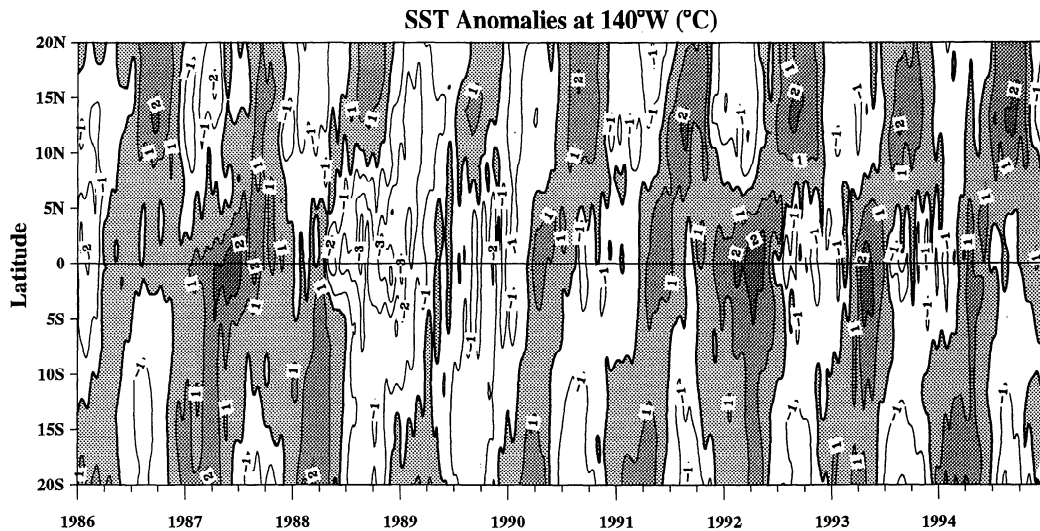


**Figure 2.** The overall SST anomalies as a function of latitude and time along 140°W. The anomalies are calculated by subtracting the time-averaged SST from the total SST of Figure 1. The contour interval is 1°C, and shading denotes positive SST anomalies.

periods of 1–3 months, seasonal includes periods of 3–11 months, annual includes periods of 11–13 months, and inter-annual includes periods of 2 years and up. The resulting seasonal, annual, and interannual SST variabilities are shown as a function of latitude and time in Figures 3a, 4a, and 5a, respectively, where the contour interval is 0.3°C and shading denotes positive SST anomalies. Intraseasonal SST variability is not shown since its latitudinal structure is similar to that of the seasonal variability. To assess meridional scales for these anomalies, the time averages of the absolute SST variations are fitted to a Gaussian function  $T(y) = T_0 \exp[-(y - y_0)^2/2L^2]$ , where the parameters  $T_0$ ,  $y_0$ , and  $L$  are determined using the method of nonlinear least squares that minimizes the devia-

tions between the data and the Gaussian function. The fitted Gaussian functions are shown as Figures 3b, 4b, and 5b.

The Gaussian function is chosen because it is the basis function for the equatorial Kelvin wave that has traditionally been used in describing ocean thermocline variability in the eastern equatorial Pacific. Visual inspection of the anomaly patterns in the vicinity of the equator also suggest that this function is appropriate. Note that because of large off-equatorial variabilities in the seasonal and annual bands these are only fitted in the vicinity of the equator as shown. Given that the SST anomalies near the equator may be described by the meridional Gaussian distribution  $T(y) = T_0 \exp[-(y - y_0)^2/2L^2]$ , the meridional scale is then defined as a length scale  $L$  at which the

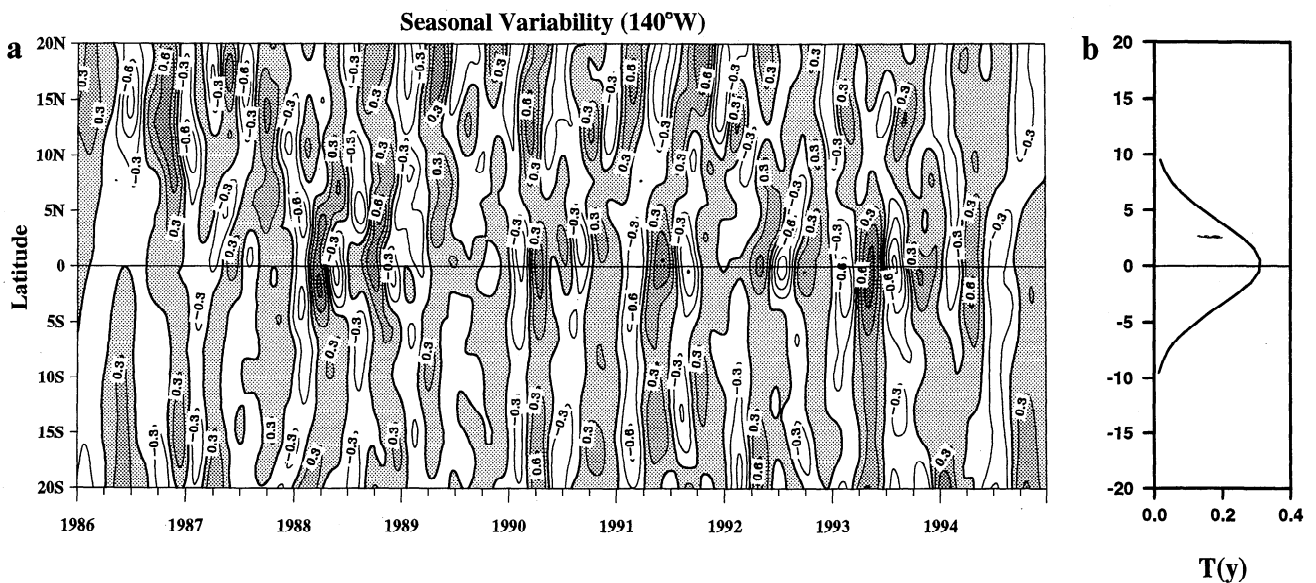


**Figure 3.** (a) The seasonal SST variability as a function of latitude and time along 140°W. The contour interval is 0.3°C, and shading denotes positive SST anomalies. (b) The result from a nonlinear least squares Gaussian distribution fit to the average absolute seasonal SST variability near the equator. The parameters in the fitted Gaussian distribution  $T(y) = T_0 \exp[-(y - y_0)^2/2L^2]$  are  $T_0 = 0.32^\circ\text{C}$ ,  $y_0 = 0.2^\circ\text{N}$ , and  $L = 3.5^\circ$ .

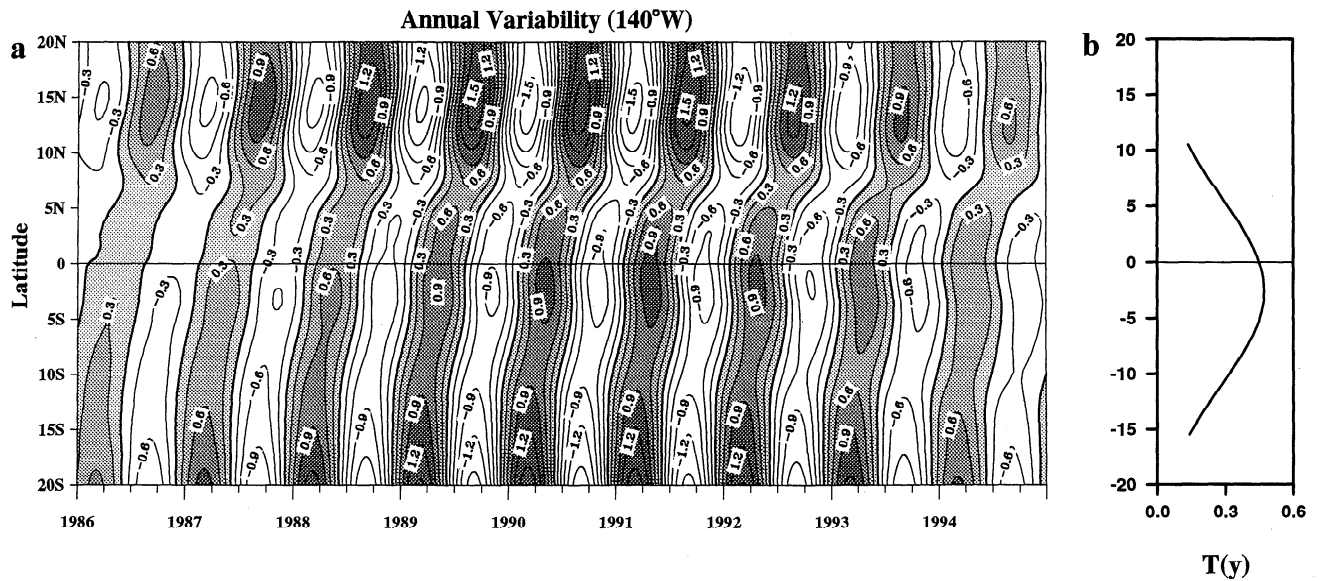


**Figure 4.** (a) The annual SST variability as a function of latitude and time along 140°W. The contour interval is 0.3°C, and shading denotes positive SST anomalies. (b) The result from a nonlinear least squares Gaussian distribution fit to the average absolute annual SST variability near the equator. The parameters in the fitted Gaussian distribution  $T(y) = T_0 \exp[-(y - y_0)^2/2L^2]$  are  $T_0 = 0.47^\circ\text{C}$ ,  $y_0 = 2.5^\circ\text{S}$ , and  $L = 8^\circ$ .

maximum amplitude ( $T_0$  at  $y = y_0$ ) decreases exponentially to  $T_0 \exp(-1/2) \approx 0.607T_0$  at  $y - y_0 = \pm L$ . For the conventional uncoupled Kelvin mode,  $y_0 = 0$ , and  $L = L_0 = (c/\beta)^{1/2}$  which, using typical values of the Kelvin wave speed  $c$ , is  $\sim 3^\circ$ .

With this definition of meridional scale, Figure 3 shows that the seasonal SST anomalies near the equator have meridional scales that are approximately equal to the oceanic equatorial Rossby radius of deformation ( $T_0 = 0.32^\circ\text{C}$ ,  $y_0 = 0.2^\circ\text{N}$ , and  $L = 3.5^\circ$ ). While not shown, a similar finding applies to SST variability on intraseasonal timescales. Thus the SST variability

on intraseasonal and seasonal timescales in the central Pacific is consistent with conventional equatorially trapped wave theory [Matsuno, 1966]. This finding conforms with the conclusions of Wang and Weisberg [1994b, 1996] that the horizontal structures and phase speeds of equatorial wave modes are unaffected by ocean-atmosphere coupling on these timescales.

The horizontal structures for the annual SST variations are distinctively different from those on intraseasonal and seasonal timescales. The off-equatorial maxima for annual SST variations occur at  $\sim 14^\circ\text{N}$  and at the southern limit of the analysis domain at  $20^\circ\text{S}$  while the near-equatorial maximum is located

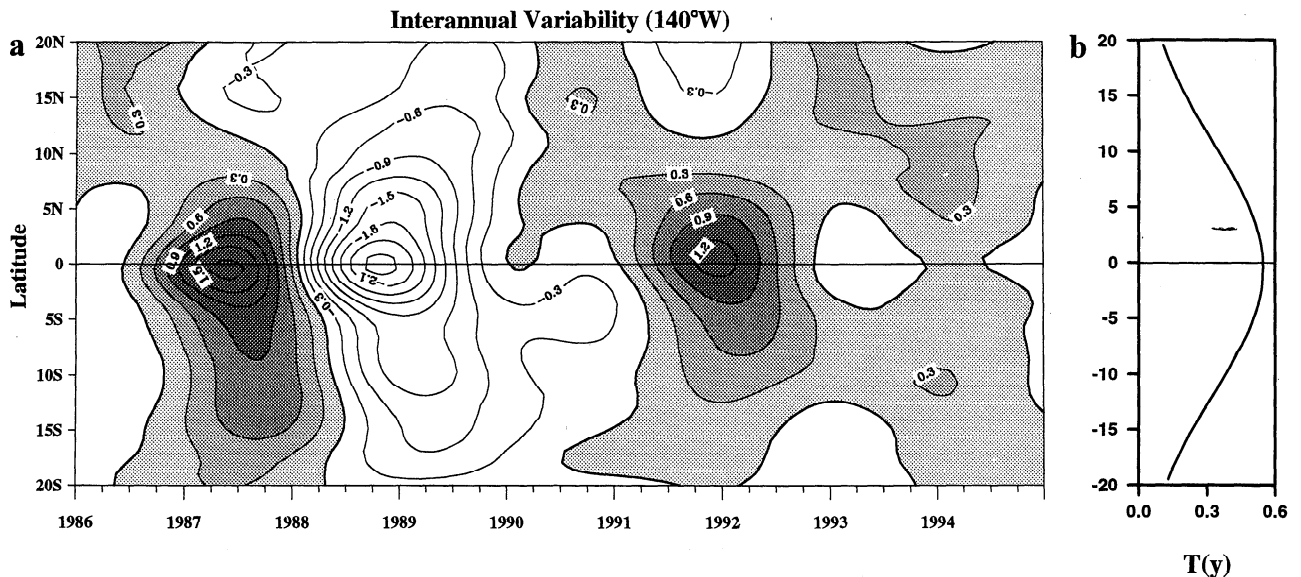


**Figure 5.** (a) The interannual SST variability as a function of latitude and time along 140°W. The contour interval is 0.3°C, and shading denotes positive SST anomalies. (b) The result from a nonlinear least squares Gaussian distribution fit to the average absolute interannual SST variability. The parameters in the fitted Gaussian distribution  $T(y) = T_0 \exp[-(y - y_0)^2/2L^2]$  are  $T_0 = 0.55^\circ\text{C}$ ,  $y_0 = 0.5^\circ\text{S}$ , and  $L = 11^\circ$ .

just south of the equator. The southernmost location is consistent with solar radiation forcing since the annual cycle in solar forcing over the analysis domain is maximum at the bounding latitudes of 20°N or 20°S. The northernmost location suggests that ocean dynamics may also be important since the maximum there does not occur at 20°N. A combination of direct solar forcing plus the effects of Ekman divergence associated with the ITCZ annual cycle might account for this. The near-equator maximum located just south of the equator reflects this large-scale hemispheric asymmetry in the annual harmonic. While the coldest water each year occurs on the equator (see Figure 1), the narrow band annual harmonic description of the annual cycle (that includes broader band components as well) shows an off-equatorial maximum. Such location is consistent with the southerly component of the southeast trade wind stress, but such a narrow band analysis, in view of Figure 1, is not complete enough to describe the annual evolution of the cold tongue. Nevertheless, fitting a Gaussian function  $T(y) = T_0 \exp[-(y - y_0)^2/2L^2]$  to the near-equatorial SST annual variability results in  $T_0 = 0.47^\circ\text{C}$ ,  $y_0 = 2.5^\circ\text{S}$ , and  $L = 8^\circ$ . The meridional scale for the annual SST variations is thus considerably larger than the intrinsic oceanic equatorial Rossby radius of deformation.

A further decrease in frequency to the interannual timescale further increases the meridional scale of the SST anomalies. This is observed in Figure 5 where the maximum SST interannual variations are centered about the equator with a broader meridional scale. Fitting a Gaussian function  $T(y) = T_0 \exp[-(y - y_0)^2/2L^2]$  to the time-averaged absolute interannual SST variability results in  $T_0 = 0.55^\circ\text{C}$ ,  $y_0 = 0.5^\circ\text{S}$ , and  $L = 11^\circ$ . A similar result was also obtained by performing an empirical orthogonal function analysis in the frequency domain, suggesting that meridional scale broadening is a property of observed SST in the central Pacific.

#### 4. Summary and Discussion

Nine years of a high-resolution OI SST product, which includes in situ (ship and buoy) SST data, satellite SST retrievals, and sea-ice coverage data [Reynolds and Smith, 1995], were used to study the frequency dependence of the meridional length scales for the coupled ocean-atmosphere system. The analyses focused on the latitudinal structures in the central Pacific at 140°W for SST anomalies varying from intraseasonal to interannual timescales. On intraseasonal and seasonal timescales the meridional scale of the SST variations is that of the intrinsic oceanic equatorial Rossby radius of deformation. For increasing timescales (decreasing frequency) the meridional scales of the SST variations are observed to increase, such that on annual and interannual timescales they are much larger than the oceanic equatorial Rossby radius of deformation. This observed frequency dependence of meridional scales for the coupled tropical ocean-atmosphere system is consistent with the analytical findings of Wang and Weisberg [1994b, 1996]. These observations of meridional scale broadening are also consistent with results from numerical models of the coupled ocean-atmosphere system [e.g., Zebiak and Cane, 1987; Barnett et al., 1991; Chao and Philander, 1993; Latif and Barnett, 1995].

Conceptually, for a coupled ocean-atmosphere system with two intrinsically different meridional scales the meridional scale of coupled equatorial modes should take on an intermediate value between the scales of the ocean and the atmosphere. A physical explanation for the increase in meridional

scale of the coupled ocean-atmosphere system follows from the coupling-induced wind stress curl in the vorticity equation. Without wind stress curl (or for the uncoupled case), conservation of absolute vorticity requires that the meridional component of velocity tends to zero at low frequency. This leaves the intrinsic oceanic equatorial Rossby radius of deformation as the meridional scale which is determined by only two parameters related to the Earth's rotation and ocean's buoyancy. By including wind stress curl as an external torque, absolute vorticity is not conserved and the meridional component of velocity tends toward a slowly varying Sverdrup balance. Coupling-inducing wind stress curl adds an additional degree of freedom to the system, and the meridional scale is then determined by the Earth's rotation and the ocean's buoyancy and ocean-atmosphere coupling. The ocean-atmosphere coupling broadens the meridional scale by altering the meridional slope of the thermocline through the wind stress curl.

The argument also can be shown mathematically by substituting the solutions of coupled ocean-atmosphere wave modes of Wang and Weisberg [1996] into the vorticity equation resulting in the dispersion relationship and demonstrating how the wind stress curl modifies the dispersion relationship. Without the ocean-atmosphere coupling, the dispersion relationship is reduced to that of Matsuno [1966]. The ocean-atmosphere coupling modifies the dispersion relationship of equatorial modes by adding another intrinsic parameter and then reducing the phase speeds. Since meridional scales of the coupled equatorial modes depend upon the phase speeds, reduction of the phase speeds due to the ocean-atmosphere coupling increases meridional scales. As an example, the meridional eigenfunctions for eastward propagating modes of Wang and Weisberg [1996] are in form of  $\exp[-\beta\omega_r/(2kc^2)y^2]$ , where  $\beta$  is the gradient in planetary vorticity,  $\omega_r$  is the real part of the frequency,  $k$  is the zonal wave number, and  $c$  is the conventional oceanic Kelvin wave speed. Therefore the meridional scale for these coupled modes can be expressed as  $L = (kc^2/\beta\omega_r)^{1/2} = L_0(c/c_c)^{1/2}$ , where  $L_0 = (c/\beta)^{1/2}$  is the oceanic equatorial Rossby radius of deformation and  $c_c = \omega_r/k$  is the modified phase speed of coupled modes from the dispersion relationship which includes the ocean-atmosphere coupling. If the ocean-atmosphere coupling does not change phase speed (i.e.,  $c_c = c$ , at high frequency or for uncoupled case), the coupled equatorial modes keep the oceanic equatorial Rossby radius of deformation  $L_0$  as their meridional scale. However, the ocean-atmosphere coupling reduces phase speeds of the coupled modes at low frequency. Reducing the phase speed of coupled equatorial wave modes (i.e.,  $c_c < c$ ) by ocean-atmosphere interaction increases the meridional scale of the coupled wave modes beyond that of the oceanic equatorial Rossby radius of deformation ( $L > L_0$ ). Previous coupled numerical model results and observations show that low-frequency oscillations within the equatorial waveguide do propagate slower than the oceanic Kelvin wave speed, consistent with the findings herein.

**Acknowledgments.** The authors would like to thank R. W. Reynolds at the NOAA National Centers for Environmental Prediction (NCEP) for providing the SST data upon which our analyses were based and W. Kessler for helpful suggestions on an earlier version of the manuscript. This work was supported by the NOAA Office of Global Programs under the Pan American Climate Studies (PACS) program grant NA56GPO241.

## References

- Barnett, T. P., M. Latif, E. Kirk, and E. Roeckner, On ENSO physics, *J. Clim.*, **4**, 487–515, 1991.
- Chang, P., Seasonal cycle of sea surface temperature and mixed layer heat budget in the tropical Pacific Ocean, *Geophys. Res. Lett.*, **20**, 2079–2082, 1993.
- Chang, P., The role of the dynamic ocean-atmosphere interactions in the tropical seasonal cycle, *J. Clim.*, **9**, 2973–2985, 1996.
- Chao, Y., and S. G. H. Philander, On the structure of the southern oscillation, *J. Clim.*, **6**, 450–469, 1993.
- Hayes, S. P., P. Chang, and M. McPhaden, Variability of the sea surface temperature in the eastern equatorial Pacific during 1986–1988, *J. Geophys. Res.*, **96**, 10,553–10,566, 1991.
- Hirst, A. C., Slow instabilities in tropical ocean basin-global atmosphere models, *J. Atmos. Sci.*, **45**, 830–852, 1988.
- Kessler, W. S., Observations of long Rossby waves in the northern tropical Pacific, *J. Geophys. Res.*, **95**, 5183–5219, 1990.
- Kessler, W. S., and M. J. McPhaden, Oceanic equatorial waves and the 1991–93 El Niño, *J. Clim.*, **8**, 1757–1774, 1995.
- Latif, M., and T. P. Barnett, Interactions of the tropical oceans, *J. Clim.*, **8**, 952–964, 1995.
- Li, T., and S. G. H. Philander, On the annual cycle of the eastern equatorial Pacific, *J. Clim.*, **9**, 2986–2998, 1996.
- Matsuno, T., Quasi-geostrophic motion in equatorial areas, *J. Meteorol. Soc. Jpn.*, **2**, 25–43, 1966.
- Philander, S. G. H., D. Gu, D. Halpern, G. Lambert, N. C. Lau, and R. C. Pacanowski, Why the ITCZ is mostly north of the equator, *J. Clim.*, **9**, 2958–2972, 1996.
- Reynolds, R. W., and T. M. Smith, Improved global sea surface temperature analysis using optimum interpolation, *J. Clim.*, **7**, 929–948, 1994.
- Reynolds, R. W., and T. M. Smith, A high-resolution global sea surface temperature climatology, *J. Clim.*, **8**, 1571–1583, 1995.
- Wang, C., and R. H. Weisberg, On the slow mode mechanism in ENSO related coupled ocean-atmosphere models, *J. Clim.*, **7**, 1657–1667, 1994a.
- Wang, C., and R. H. Weisberg, Equatorially trapped waves of a coupled ocean-atmosphere system, *J. Phys. Oceanogr.*, **24**, 1978–1998, 1994b.
- Wang, C., and R. H. Weisberg, Stability of equatorial modes in a simplified coupled ocean-atmosphere model, *J. Clim.*, **9**, 3132–3148, 1996.
- White, W. B., S. E. Pazan, and M. Inoue, Hindcast/forecast of ENSO events based on redistribution of observed and model heat content in the western tropical Pacific, 1964–1986, *J. Phys. Oceanogr.*, **17**, 264–280, 1987.
- White, W. B., Y. H. He, and S. E. Pazan, Redistribution of subsurface thermal structure during the onset of the 1982–83 and 1986–87 ENSO events and the 1984–85 anti-ENSO event, *J. Phys. Oceanogr.*, **19**, 1397–1406, 1989.
- Xie, S. P., On the genesis of the equatorial annual cycle, *J. Clim.*, **7**, 2008–2013, 1994.
- Xie, S. P., and S. G. H. Philander, A coupled ocean-atmosphere model of relevance to the ITCZ in the eastern Pacific, *Tellus Ser. A*, **46**, 340–350, 1994.
- Zebiak, S. E., and M. A. Cane, A model El Niño-Southern Oscillation, *Mon. Weather Rev.*, **115**, 2262–2278, 1987.

C. Wang and R. H. Weisberg, Department of Marine Science, University of South Florida, 140 Seventh Avenue South, St. Petersburg, FL 33701. (e-mail: wang@ocg6.marine.usf.edu)

(Received October 8, 1996; revised September 9, 1997; accepted September 25, 1997.)